ELSEVIER

Journal of Power Sources 112 (2002) 596–605

JOURNAL OF POWER SOURCES

www.elsevier.com/locate/jpowsour

Pechini process-derived tin oxide and tin oxide–graphite composites for lithium-ion batteries

R. Zhang[a], Jim Y. Lee[a,*], Z.L. Liu[b]

[a]*Department of Chemical and Environmental Engineering, National University of Singapore, 10 Kent Ridge Crescent, Singapore 119260, Singapore*

[b]*Institute of Materials Research and Engineering, 3 Research Link, Singapore 117602, Singapore*

Received 12 June 2002; accepted 29 August 2002

Abstract

The Pechini process [Ceram. Bull. 68 (1989) 1002] is used to obtain fine tin oxide powders that reduce the specific volume change in Li^+ insertion and extraction reactions. The suitability of these tin oxides as active materials for negative electrodes in lithium-ion batteries is investigated. From elemental analysis, it is found that the templating polymer network is almost completely obliterated after heating at 500 °C. The best tin oxide does not exhibit extensive crystallization of tin atoms even after 30 cycles of alloying and de-alloying reactions with Li. The structure and the specific capacity of the oxides are dependent on the heat treatment and remnants of the polymeric C–H network can impose an unfavorable outcome. A capacity of 600 mAh g^{-1}, which is unchanged for 30 cycles, can be obtained from tin oxide heat treated at 1000 °C. Composites of graphite and SnO_2 are also prepared and exhibit synergistic interactions between graphite and tin oxide which are similar to those reported previously [Electrochem. Solid State Lett. 3 (2000) 167].

Keywords: Tin oxide; Graphite; Anode; Lithium-ion battery; Pechini process

1. Introduction

Lithium alloy anodes for lithium-ion batteries had been investigated in some detail before carbonaceous materials were widely accepted for the same application. An obvious advantage of Li^+ insertion into a compatible metal is the high packing density that can be achieved in Li alloys. Unfortunately, a large specific volume change (usually by a factor of two or three) occurs in the host matrix during the insertion and removal of Li [3]. This causes rapid anode disintegration under the induced mechanical stress. Carbonaceous materials have much smaller expansion and contraction problems, but are beset with a relatively low packing density compared with the Li-metal alloys.

One way to contain the volume changes during Li^+ insertion and extraction is to embed the active material in a cushioning medium which maintains particle connectivity, even after pulverization. The medium can be electrochemically active or inactive. A well-known example is the amorphous tin composite oxide (ATCO) anode from Fuji Film [4].

Tin-based oxides have theoretical volumetric and gravimetric capacities that are, respectively, four and two times that of carbon. There is, however, a substantial loss of charge and Li^+ in the first cycle due to electrochemical reduction of the oxide. According to Courtney and Dahn [5], the Li_2O formed in the first cycle could buffer the volume change in subsequent Li reactions with Sn, and decrease the tendency of tin atom aggregation on prolonged cycling [5]. In practice, tin composite oxides have shown reduced (relative to tin), but not insignificant, capacity fading upon cycling [5–9]. This indicates that the Li_2O matrix is not completely effective in preventing tin aggregation into large coherent domains. There were also attempts to add one or more elements to tin to deliver the same benefits as cushioning Li_2O without its disadvantages. For instance, Yang et al. [10] used chemical reduction to obtain Sn–SnSb powders as active materials [10], and Mao et al. [11–13] prepared a complete series of Sn–Fe–C powders by mechanical alloying. The irreversible losses on the first cycle are lowered, but in some cases cycleability is compromised. SnO_2 has also been doped with Mo, P, and B [4,7,14,15] to hinder tin aggregation in charge and discharge reactions. It is generally believed that the ability to produce and maintain tin in high dispersion throughout charging and discharging is the key to good cycleability [7].

* Corresponding author. Tel.: +65-874-2899; fax: +65-6779-1936.
E-mail address: cheleejy@nus.edu.sg (J.Y. Lee).

0378-7753/02/$ – see front matter
PII: S0378-7753(02)00483-4

This investigation uses the Pechini process [1,16] to produce tin composite oxide materials. The Pechini process was originally developed to prepare metal oxide powders such as titanates and niobates for capacitors [16]. Recently, it has been applied to the syntheses of a number of cathode materials [17,18], as well as electroceramics such as superconducting fibers [19]. The Pechini process is based on the ability of weak polybasic acids to form chelates with cations. These chelates then undergo polyesterification when heated in a polyhydroxyl alcohol to form a solid polymer resin in which the cations are uniformly dispersed. The resin is subsequently calcined at lower temperatures to yield fine oxide particulates. With this method, we hope to produce very fine powders of tin oxide with improved electrochemical properties. The issue of irreversibility capacity loss may then be addressed through compounding with a capacity compensating material such as $Li_{2.6}Co_{0.4}N$ [20].

2. Experimental

2.1. Materials preparation

The 0.02 M citric acid (Merck, 99.5%) and 0.015 M $SnCl_2{\cdot}H_2O$ (Merck, 99%) were added to 50 ml of distilled water. The mixture was vigorously stirred for 3 h to obtain a clear solution. The 0.015 M of ethylene glycol (99.9%) was then introduced and the mixture heated. A yellow gel slowly formed which eventually turned into a block of solid. The solid was ground into a fine powder and heated for 3 h in air in a tube furnace at 300, 500, 700, and 1000 °C, respectively. The procedure was also repeated by dispersing 1.5 g graphite (KS6, TimCal, BET surface area = 19 $m^2\ g^{-1}$) in the solution at the beginning to produce tin oxide–graphite composite precursors. Those too were heated for 3 h in air at 300 and 500 °C, respectively.

2.2. Materials characterizations

The tin oxide samples were examined by scanning electron microscopy (SEM) at 15 kV and 1000× magnification in a Philips XL30 instrument. Determination of crystal structure was performed primarily by means of powder X-ray diffraction (XRD) using a Siemens D6000 diffractometer, Cu Kα radiation, and a scan range of 20–70°. The carbon contents of samples heated at different temperatures were determined by means of a Perkin-Elmer 2400 CHN elemental analyzer.

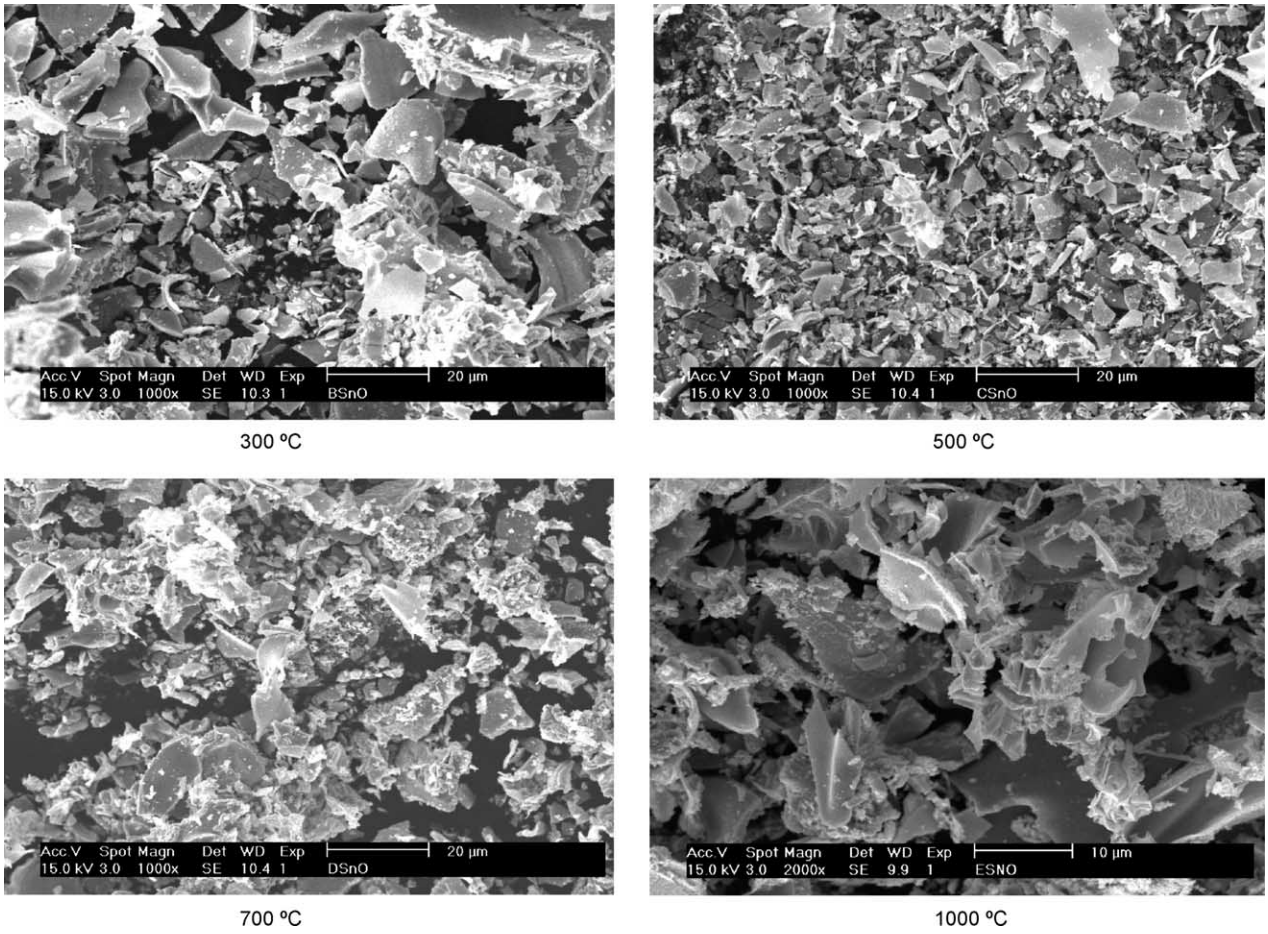

Fig. 1. Electron micrographs of Pechini process-derived SnO_2 precursors after firing at different temperatures.

2.3. Electrochemical tests

The tin oxides were made into slurries containing 80 wt.% oxide powder, 10 wt.% carbon black, and 10 wt.% polyvinlidene di-fluoride (PVDF) in *N*-methyl pyrolidinone (NMP); and were coated on high-purity copper foils (thickness: 25 μm). For the tin oxide–graphite composites, the composition of the slurries was changed to 88:2:10 (active material:carbon black:PVDF). The coated foils were dried in vacuum overnight at 100 °C and pressed between stainless-steel plates at 1.4×10^7 Pa before they were cut into circular discs of 11 mm diameter. Electrochemical cells were assembled using tin oxide as the positive electrode, a polypropylene microporous separator, a electrolyte of 1 M $LiPF_6$ in a 50:50 (v:v) mixture of ethylene carbonate (EC) and diethyl carbonate (DEC), and a lithium foil negative electrode (thickness: 0.75 mm). Cell assembly was carried out in an argon-filled glove box where both moisture and oxygen were kept below 1 ppm each. The cells were cycled with a Maccor series 4000 battery tester between 5 mV and 1 V using a constant current density of 75 mA g^{-1} (or 0.4 mA cm^{-2}) at a constant temperature of 25.0 ± 0.1 °C.

For investigation of the Li^+ insertion and extraction mechanisms, three cells were charged[1] to 1.2, 0.8, and 5 mV, respectively, from open-circuit. The fourth cell was charged to 5 mV and then discharged to 1 V using a constant current density of 75 mA g^{-1} (0.4 mA cm^{-2}). The cells were then dismantled in a glove box and laboratory wipes were used to remove excess electrolyte from the electrode surface. The electrodes were covered with Mylar films and analyzed by ex situ X-ray diffraction.

3. Results and discussion

Electron micrographs of the products from the Pechini process after firing at 300, 500, 700, and 1000 °C for 3 h are shown in Fig. 1. All samples were morphologically alike, and showed prismatic-shaped flakes with noticeable irregularity. Chemical analysis reported virtually no trace of carbon and hydrogen for samples heated to 500 °C and higher; and hence the composition is basically pure SnO_2. The free volume in these materials is likely to increase with the heat-treatment temperature, when residual carbon and hydrogen from the precursor are progressively burnt off. The more open structure serves to buffer against the volume change in lithium insertion and extraction reactions, and also provides a facilitated pathway for the transport of lithium ions. Experimentally, the high-temperature samples were more cycleable and had higher specific capacities (see later).

The diffraction patterns of the products from the Pechini process are presented in Fig. 2. All peaks in the scan range 20–70° can be indexed to the three major peaks of SnO_2, namely, the (1 1 0), (1 0 1), and (2 1 1) diffractions. The peak intensities increase slightly with increase in heat-treatment temperature. This demonstrates the stability of the smaller grains.

The Pechini process is a sequential process that consists of the following reactions:

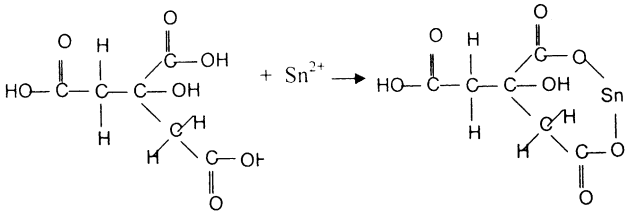

(1)

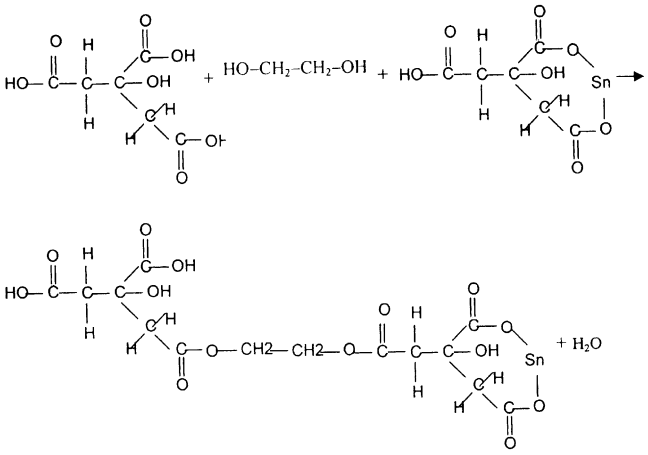

(2)

The first step is chelate formation, which initiates the uniform distribution of tin ions. The chelates undergo polyesterification with ethylene glycol to grow into a polymer network. Water in this condensation reaction is removed by heating, and leaves a solid resin behind which keeps tin in the original state of high dispersion. The resin is then calcined at a suitable temperature to yield fine particulates of oxides. The polymeric structure is broken down in the firing process and; releases tin as SnO_2. This method makes it simple to obtain phase-pure, ultrafine powders in a few hours at a suitable temperature. For battery applications, it has been used in the production of $LiMn_2O_4$ spinels [17,18,21].

The effect of heat-treatment temperature on the specific capacity of various tin oxides prepared by the Pechini process is shown in Table 1. It is clear that a greater capacity is obtained at a higher temperature. This indicates that only tin atoms in the form of SnO_2, and totally detached from the extensive polymeric network, are reactive towards Li^+. This is verified experimentally by the total absence of any capacity for the non-heat-treated sample where Sn is fully networked. The non-conducting nature of the C–H network hinders the flow of compensating electrons in the Li^+ insertion and extraction reactions, and results in no

[1] Charge and discharge in this article refers to Li^+ insertion and extraction, respectively, as would be the case if tin oxide was coupled to a transition metal oxide to form a working lithium-ion battery.

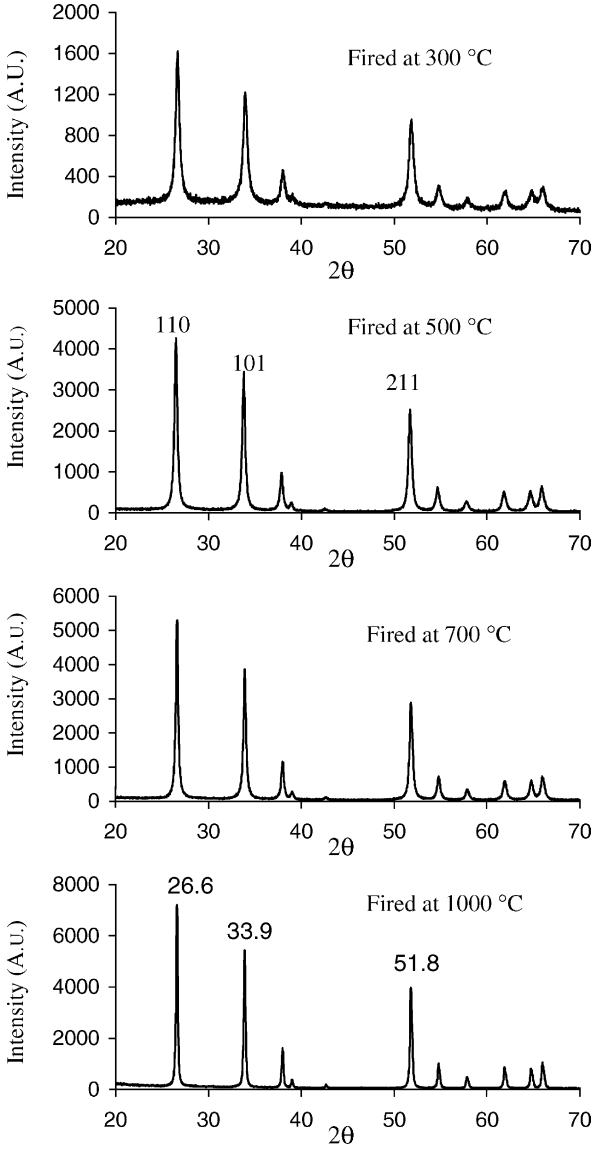

Fig. 2. Evolution of SnO_2 X-ray diffraction patterns at different heat-treatment temperatures.

observable capacity. The same heat-treated sample also produces charging problems in SEM examinations because of its lack of electrical conductivity. Pyrolysis raises the electron conductivity to at least the level of semi-conducting SnO_2. The gentle removal of the polymeric network prevents the coalescence of the tin oxide particles, which preserves some of the open structures present in the precursor network. The presence of free volume is reflected by the increase in BET surface area with temperature until about 1000 °C. The decrease in the BET surface area thereafter is the result of particle sintering becoming more prevalent. Particle-size measurements by laser light scattering show all the particles to be in the same size range (d_{50} ~0.6 μm). Hence, the increase in BET surface area is due to the increase in the voidage of the particles.

The charge and discharge curves of the tin oxides heat-treated at different temperatures is shown in Fig. 3. There is a plateau in the charging curves around 1 V, which corresponds well with the reported formation of Li_2O and Sn metal [5]. Except for the 300 °C treated sample, all other curves have a similar appearance. This is perhaps caused by the low SnO_2 content in the 300 °C sample (78%) compared with the others (~100%). Chemical analysis shows that the 300 °C sample has a high residual carbon content, which indicates the presence of remnants of the polymeric network. It has been reported [22–24] that Li–Sn alloys only exist below 0.8 V, and hence Sn is likely to be reformed in the discharge cycles around 0.9 V. At discharge potentials higher than 1.3 V, some Li_2O decomposition may take place and result in deterioration of cycle-life [7]. Given these possibilities [5,22], the discharge limit was capped at 1 V in all the experiments reported here.

The theoretical specific capacities of Sn, SnO, and SnO_2 are 1000, 880, and 780 mAh g^{-1}, respectively, based on the assumption that each tin atom can accommodate up to a maximum of 4.4 Li atoms. Most work on pristine SnO and SnO_2 [25–28] has reported specific capacities lower than the theoretical values when the discharge was limited to 1 V. Even in cases where the discharge cut-off was raised to 2 V [6], only 3.5 Li atoms per tin atom could be recovered. Some of the previous studies on Li^+ storage in tin oxides are summarized in Table 2. These numbers have been extracted from the charge and discharge curves in the original reports and represent the high end of the capacities. All of them are substantially lower than the theoretical values. Capacity retention is very poor for some of them. In the study by Courtney and Dahn [5], the capacity decreases from the first cycle to the second cycle by 100 mAh g^{-1} for SnO, and by 200 mAh g^{-1} for SnO_2. The performance for the best sample examined Kim et al. [30] was a reversible capacity of 569 mAh g^{-1} (0–1.5 V) with a fade rate of 0.4% per cycle for 10 cycles. By comparison, the 1000 °C sample in this

Table 1
Specific capacities of various SnO_2 samples, produced by the Pechini process, in Li^+ insertion and removal reactions

Sample	Temperature (°C)	Average reversible specific capacity (mAh g^{-1}) 0–1 V	Average reversible specific capacity (mAh g^{-1}) 0–2 V	Carbon content (wt.%)	BET (m^2 g^{-1})
A	300	330	470	22	1.88
B	500	480	820	0.1	8.53
C	700	510	818	0.1	8.90
D	1000	600	840	0.07	5.45

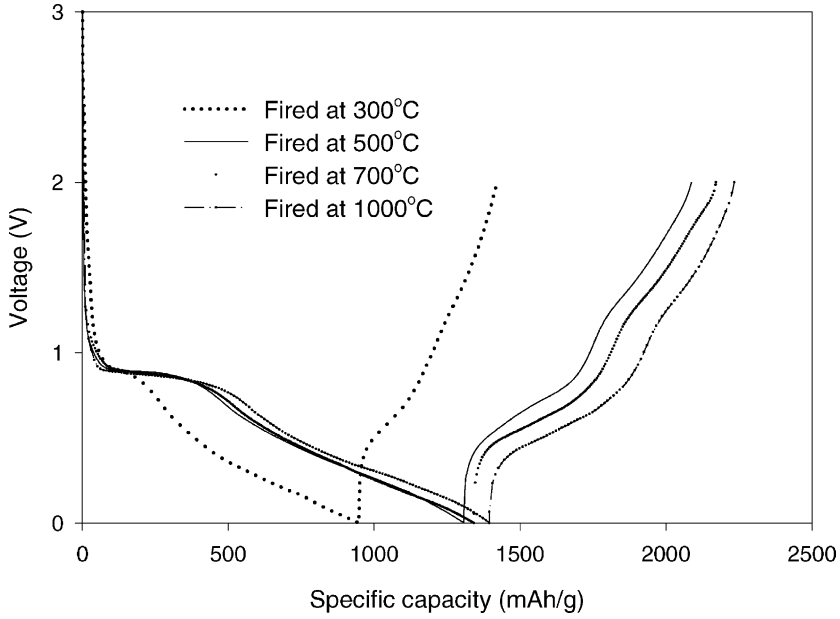

Fig. 3. First-cycle charge and discharge curves of SnO_2 prepared by Pechini process and fired at different temperatures.

Table 2
Practical specific capacities of SnO_2 reported in the literature

Oxide type [references]	Li^+ extraction up to 1 V (specific capacity in mAh g^{-1})	Li^+ extraction up to 2 V (specific capacity in mAh g^{-1})	Current density
SnO_2 [29]	~400	~600	0.125 mA cm^{-2}
SnO_2 [19]	~450 (0–1.15 V)		
SnO_2 [30]	760 (0–1.5 V)		
SnO_2 [5]	~600	~850	18.6 mA g^{-1}
This work	~600	~850	0.4 mA cm^{-2} or 70 mA g^{-1}

study was able to sustain a high reversible capacity of 624 mAh g^{-1} for 26 cycles at a fade rate of 0.2% per cycle, all within a narrower voltage range of 0–1 V.

The application performance was further enhanced by increasing the conductivity of the electrode. The charge and discharge curves of the tin oxides fired at 700 °C are shown in Fig. 4a. The electrode was formulated according to the normal practice of SnO_2:carbon black = 8:1.[2] The charge–discharge profiles of the same material with more carbon black added during formulation (SnO_2:carbon black = 1:1) are presented in Fig. 4b. For the first seven cycles, the normally formulated SnO_2 could only exchange three Li atoms per Sn atom, whereas sample enhanced with the carbon black allowed 4.1 Li atoms to be exchanged, i.e. closer to the theoretical limit of 4.4. The charge and discharge plateaux are also flatter in appearance. As the 1:1 mixture is not an appropriate formulation from the utilization point of view, tin oxides were mixed according to the 8:1 formulation throughout the remaining experiments for a more realistic assessment of the material performance.

[2] Carbon black has little reversible capacity for Li storage.

The cycleability of SnO_2 prepared by the Pechini process is compared in Fig. 5 with SnO_2 prepared from $SnCl_2$ hydrolysis [2] (with 10 wt.% carbon black and 10 wt.% PVDF). The Pechini SnO_2 treated at 1000 °C for 3 h has the highest and most stable discharge capacity (620 mAh g^{-1}) and shows little capacity fading over 30 cycles. For SnO_2 treated at 700 °C, the initial capacity of 500 mAh g^{-1} decreases to 420 mAh g^{-1} in the same number of cycles. The sample treated at 500 °C also experiences a capacity decrease from 480 to 400 mAh g^{-1}, and the 300 °C treated sample, from 320 to 290 mAh g^{-1} in 30 cycles. It is generally believed that the key to good cycle-life lies with control of Sn particle size and the prevention of the Sn particles from agglomerating into large clusters. The Pechini reactions enable the initial establishment of a high Sn dispersion. The encapsulation of Sn atoms by the interpenetrating polymeric network effectively limits the sintering agglomeration of tin even as the polymer network is being progressively removed by firing. The end result is a very fine SnO_2 powder where the small particle size increases the energy barrier to agglomeration. The SnO_2 powders prepared by conventional hydrolysis have no such protection

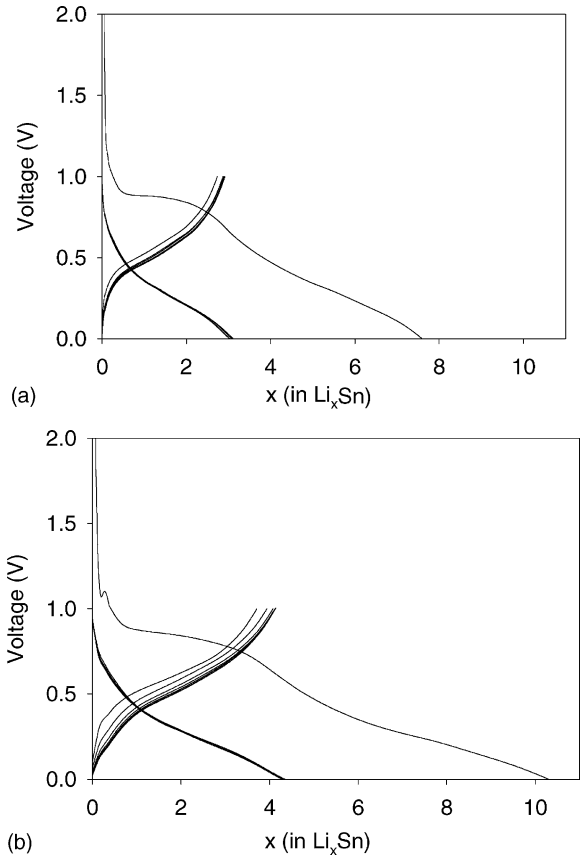

Fig. 4. Charge and discharge curves of sample C during first seven cycles: (a) SnO_2:carbon black = 8:1; and (b) SnO_2:carbon black = 1:1.

during its inception and hence exhibit substantial capacity fading from 400 to 300 mAh g^{-1} in 30 cycles.

Despite the promising cycling behavior, especially for the sample heat-treated at 1000 °C, the tin oxides are beset with substantial irreversible capacity losses in during first cycle. From the data in Table 3, the lower coulombic efficiency in 0–1 V window is due mainly to incomplete Li extraction at the 1 V level. The discharge capacity is about 20% lower than the theoretical value of 780 mAh g^{-1}. If decomposition of SnO_2 during the first cycle is main cause of the irreversibility, then the loss should amount to 700 mAh g^{-1}. The measured values of the first-cycle losses are higher, viz. about 800–900 mAh g^{-1} (0–1 V). The loss is smaller (~500 mAh g^{-1}), however, if the voltage range is widened to 0–2 V. This shows that some Li is deeply seated and can only be extracted by high negative potentials. Extraction at 1.3 V, and beyond, might also cause the decomposition of Li_2O, which contributes to the apparent reduction in irreversibility capacity loss in the 0–2 V range.

The effect of particle size on retarding the aggregation of tin atom can also be witnessed by X-ray diffraction. The diffraction pattern of the 700 °C treated SnO_2 after charging (Li^+ insertion) to 0.8 V in the first cycle is shown in Fig. 6a. The peaks at 25.5 and 28° are background signals from the Mylar film. The peaks at 33.82 and 51.6° are due to SnO_2, but another peak at 26° is masked by the carbon peak from the Mylar cover which protected the sample from oxidation during measurements. The intensity of the 25.5° peak decreases upon lithium insertion because of the

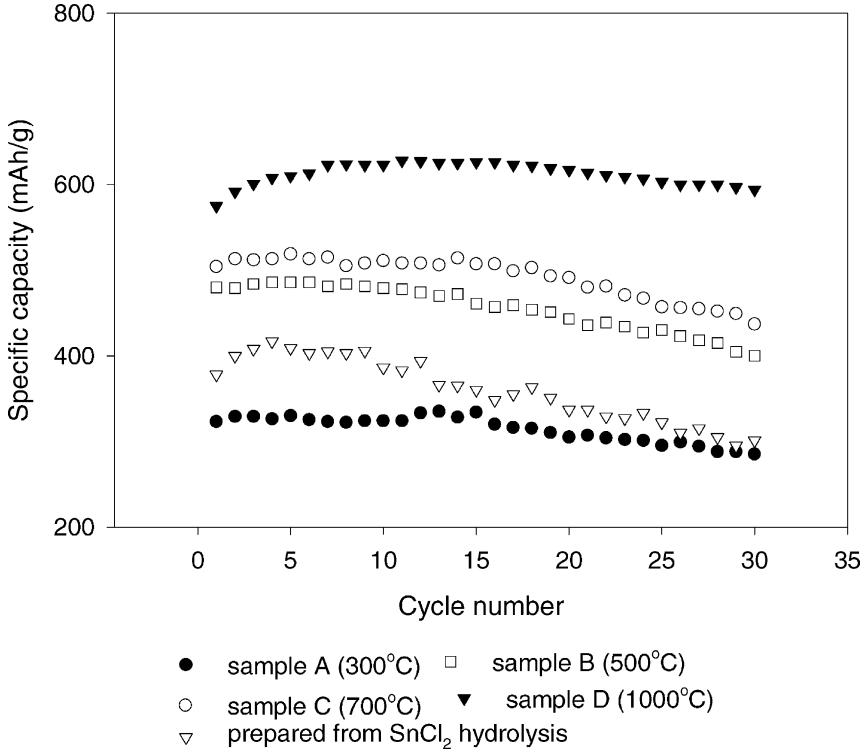

Fig. 5. Comparison of cycleability of different SnO_2 samples (test conditions: 0.4 mA cm^{-2}; 0–1 V).

Table 3
Coulombic efficiency in 0–1 and 0–2 V voltage windows

Sample	0–1 V in first cycle		0–2 V in first cycle	
	Intercalation/de-intercalation (mAh g^{-1})	Columbic efficiency (%)	Intercalation/de-intercalation (mAh g^{-1})	Columbic efficiency (%)
A	950/375	39	1015/472	46.5
B	1268/457	36	1312/820	62.5
C	1400/504	36	1369/846	61.8
D	1390/575	41	1331/840	63.1

decomposition of SnO_2 to Sn and Li_2O. This was also observed by Courtney and Dahn [5] in charging SnO_2 to 1 V in the first cycle. In this work, a remnant of SnO_2 was still visible after charging to 0.8 V, and metallic tin was not detectable by X-rays. This is perhaps due to the fact that of the tin atoms have a very small size and are therefore not X-ray coherent. The diffraction pattern after charging to 5 mV is shown in Fig. 6b. All X-ray signatures of SnO_2 disappear completely, and the peak at 38.3° corresponds well to Li–Sn alloy [31]. The diffraction pattern of the same material discharged to 1 V after being previously charged to 5 mV is shown in Fig. 6c. As lithium is extracted during discharge, the peak pertaining to the Li–Sn alloy disappears, and the twin peaks at 31 and 32° are indications of the formation of tin metal. The degree of crystallization as perceived by X-rays is, however, very low. A sample in the discharged state after 30 cycles has also been analyzed by X-ray diffraction. While the presence of Li and Sn as independent entities is expected at this stage, it was not possible to identify their presence by X-rays. This is indicative of the resistance to tin agglomeration in SnO_2 prepared by the Pechini process. This observation differs from that made in other work [2,12] where the presence of tin could be more easily detected in the first cycle, probably as a result of uninhibited particle growth. Retoux et al. [28] reported that the size of the tin crystallites formed during the first cycle could increase from 40 to 110 nm after 500 cycles.

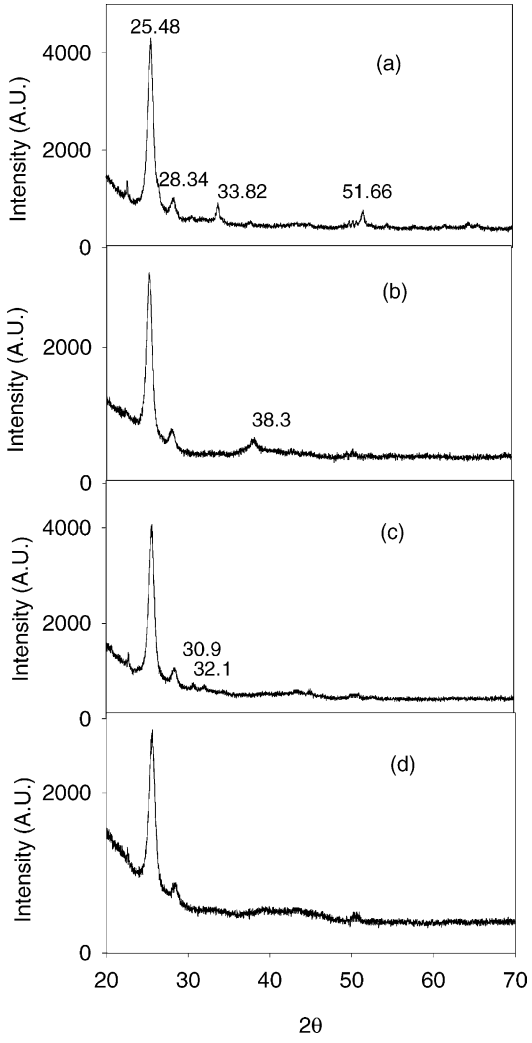

Fig. 6. X-ray diffraction patterns of SnO_2 at different stages of charge and discharge in first cycle: (a) after charging to 0.8 V; (b) after charging to 5 mV; (c) after discharging to 1 V; and (d) in discharged state after 30 cycles.

We observed previously [2] synergistic interactions between graphite and SnO_2 when the latter was highly dispersed in the former. Some graphite–SnO_2 composites have also been prepared in the present work to determine the generality of the previous observation. Powder diffraction patterns of graphite–tin oxide composites prepared by the Pechini process at 300 °C (EA) and 500 °C (EB), respectively, are presented in Fig. 7. The concentration of SnO_2 in each of these samples was found to be 2 wt.% from ICP measurements. As expected, the X-ray signal of crystalline SnO_2 increases with increase in heat-treatment temperature, as shown by the generally stronger diffractions in the EB sample. The diffraction peak at 26° contains a large contribution from the graphite (0 0 2) plane, and hence its intensity relative to other SnO_2 diffractions is higher than the level indicated in Fig. 2. No crystalline phases other than SnO_2 that could be detected by X-ray diffraction.

The cycleability of EA and EB is compared in Fig. 8. It is immediately apparent that adding tin oxide to graphite by the Pechini process has produced no sustainable improvement in cycle-life. This is possibly due to the partial coverage of graphite particles by the polymeric precursor network which could not be removed by low temperature burn-off at 300 °C. Compared with graphite, the polymeric network has slower kinetics for Li^+ transport and hence the capacity is

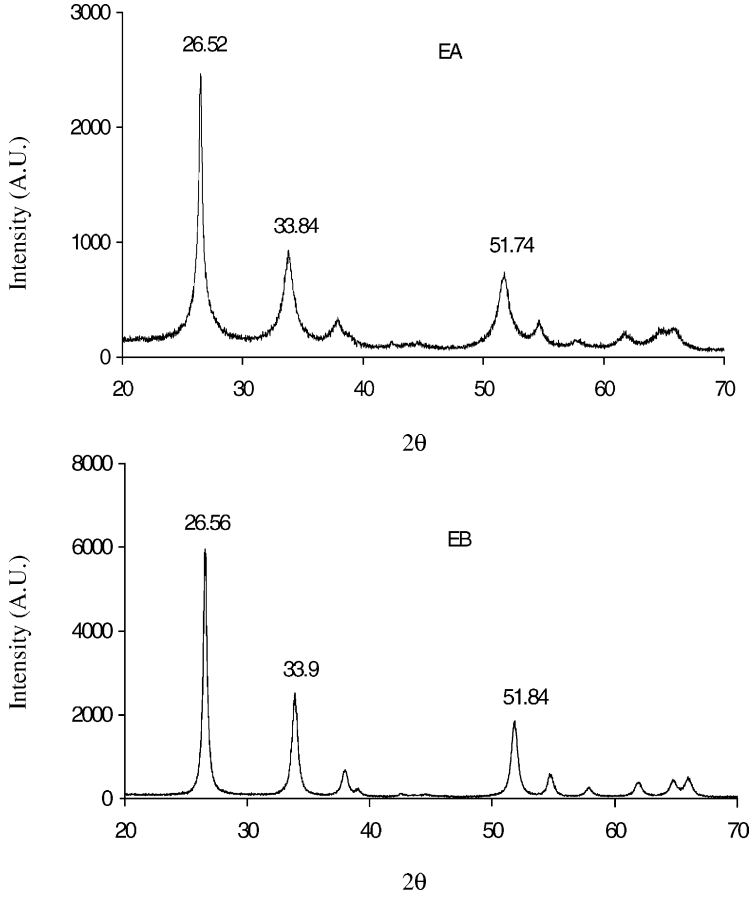

Fig. 7. X-ray diffraction patterns of graphite–SnO_2 composites prepared by Pechini process.

adversely affected. The specific capacity of EB is significantly better because the higher burn-off temperature of 500 °C results in a more complete removal of the precursor network. Higher heat-treatment temperatures were not attempted because of the possibility of graphite oxidation and irreproducible modifications of the carbon surfaces.

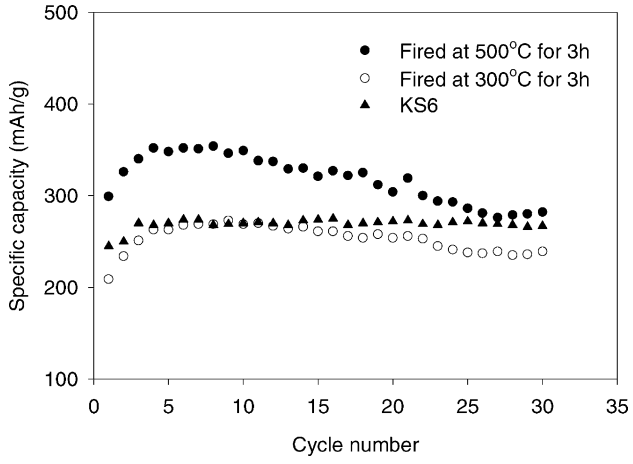

Fig. 8. Cycleability of graphite and graphite–SnO_2 composite prepared at different temperatures (test conditions: 0.4 mA cm^{-2} (75 mA g^{-1}); 0–1 V).

Scanning electron micrographs of EA, EB and a pristine graphite sample (KS6) are shown in Fig. 9. After treatment by the Pechini process, the free space between the graphite flakes is filled with bridging polymeric materials (Fig. 9b and c). The bridges are not removed by heating to 300 °C and the graphite particles remain highly agglomerated. The diffusion of Li-ions into and from the graphite interior is likely to be hindered and therefore result in low capacities. Increasing the heat-treatment temperature to 500 °C removes a good part of the polymeric bridges, as can be seen by the more open structure in the powder shown in Fig. 9c. Accordingly, Li-ion transport is less hindered in this case, and accounts for the experimental increase in capacity.

The data in Table 4 highlight difference between the specific capacities of EA and EB, where SnO_2 is deposited on graphite by the Pechini process, and the specific capacities of mechanical mixtures of SnO_2 obtained by the Pechini process and graphite with the same overall compositions; at 0.4 mA cm^{-2} between 5 mV and 1 V.

The specific capacities of Pechini process-derived SnO_2 treated at 300 and 500 °C is 330 and 480 mAh g^{-1}, respectively (Table 1). The data in Table 4 show that the capacity of graphite is not improved by mechanical mixing with SnO_2 because of the small amount (2 wt.%) of tin oxide added (samples MM1 and MM2). The mixtures delivered only the

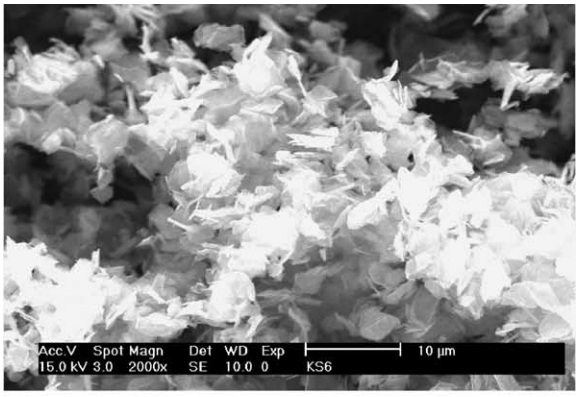

Pristine KS6

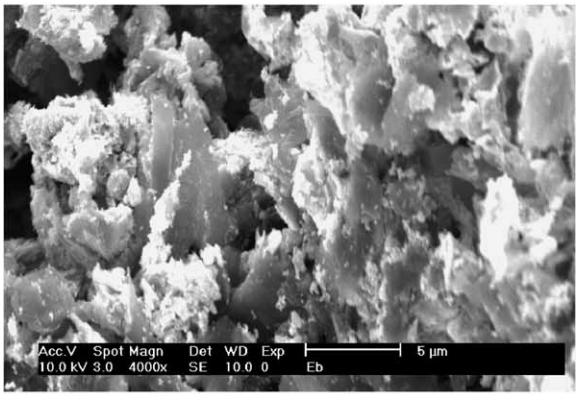

EA

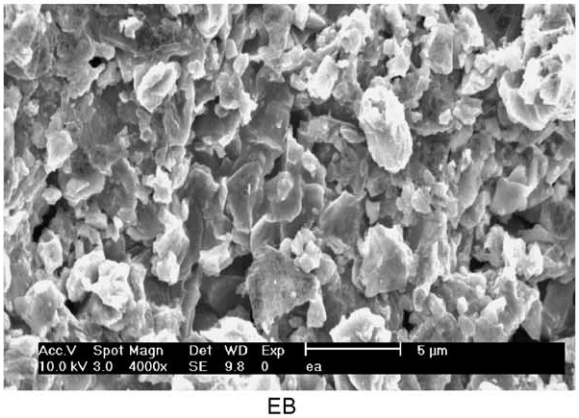

EB

Fig. 9. Electron micrographs of samples EA, EB and pristine graphite KS6.

Table 4
Specific capacities (mAh g^{-1}) of SnO_2–graphite composites, mechanical mixtures of SnO_2 and graphite, and graphite

SnO_2 (wt.%)	Designation	Capacity (mAh g^{-1})
2	EA (300 °C)	270
2	EB (500 °C)	350
0	KS6	270
2	MM1[a]	260–270
2	MM2[b]	260–270

[a] 2 wt.% Pechini process-derived SnO_2 fired at 300 °C and 98% KS6.
[b] 2 wt.% Pechini process-derived SnO_2 fired at 500 °C and 98% KS6.

typical capacity of graphite (sample KS6). By contrast, the EB sample, despite the same low SnO_2 concentration, increases the graphite capacity by as much as 30%. This can be attributed to the good dispersion of SnO_2 in graphite by the Pechini process so that the former can be fully utilized electrochemically. More importantly, if it is assumed that SnO_2 and graphite contribute independently to the overall capacity, the composite will have a capacity of 280 mAh g^{-1} instead of the 350 mAh g^{-1} observed here. Hence, the synergistic interactions between highly dispersed tin oxide and graphite, which were first reported in our previous work [2], is again evident here. The effect appears to require only a high dispersion of the tin oxide phase and is largely independent of the synthesis details that lead to high dispersion.

4. Conclusions

Fine powders of tin oxide are obtained from Pechini synthesis followed by heat treatment above 500 °C. The materials are resistant to tin atom agglomeration and exhibited good cycle-life in rechargeable Li batteries. It is speculated that their small size and the presence of intervening free volumes between them provide an effective cushion against the specific volume change that accompanies Li insertion and extraction reactions. Tin oxide prepared by the Pechini process and fired at 1000 °C, show a reversible capacity of 600 mAh g^{-1} between 0 and 1 V which is nearly invariant for 30 cycles, without any indication of tin particle growth. Graphite–tin oxide composites have also been prepared and the synergistic interactions previously observed [2] are again evident. This indicates the merits of a high dispersion of tin oxide in graphite as a viable means to increase the capacity of graphite beyond its theoretical limit.

References

[1] P.A. Lessing, Ceram. Bull. 68 (1989) 1002.
[2] J.Y. Lee, R.F. Zhang, Z.L. Liu, Electrochem. Solid State Lett. 3 (2000) 167.
[3] R. Nesper, Prog. Solid State Chem. 20 (1990) 1.
[4] Y. Idota, T. Kubota, A. Matsufuji, Y. Maekawa, T. Miyasaka, Science 276 (1997) 1395.
[5] I.A. Courtney, J.R. Dahn, J. Electrochem. Soc. 144 (1997) 2045.
[6] H. Li, X. Huang, L. Chen, J. Power Sources 81 (1999) 335.
[7] I.A. Courtney, J.R. Dahn, J. Electrochem. Soc. 144 (1997) 2943.
[8] A. Hightower, P. Delcroix, G.L. Caer, C.K. Huang, B.V. Ratnakumar, C.C. Ahn, B.J. Fultz, J. Electrochem. Soc. 147 (2000) 1.
[9] S. Machill, T. Shodai, Y. Sakurai, Y.J. Yamaki, J. Power Sources 73 (1998) 216.
[10] J. Yang, M. Wachtler, M. Winter, J.O. Besenhard, Electrochem. Solid State Lett. 2 (1999) 161.
[11] O. Mao, R.A. Dunlap, J.R. Dahn, J. Electrochem. Soc. 146 (1999) 405.
[12] O. Mao, J.R. Dahn, J. Electrochem. Soc. 146 (1999) 414.
[13] O. Mao, J.R. Dahn, J. Electrochem. Soc. 146 (1999) 423.
[14] J. Morales, L. Sanchez, J. Electrochem. Soc. 146 (1999) 1640.
[15] I.A. Courtney, W.R. Mckinnon, J.R. Dahn, J. Electrochem. Soc. 146 (1999) 59.

[16] M.P. Pechini, US Patent No. 3,330,697 (11 July 1967).
[17] W. Liu, G.C. Farrington, F. Chaput, B. Dunn, J. Electrochem. Soc. 143 (1996) 879.
[18] Y. Han, H. Kim, J. Power Sources 88 (2000) 166.
[19] S.C. Zhang, G.L. Messing, W. Huebner, M.M. Coleman, J. Mater. Res. 5 (1990) 1806.
[20] J. Yang, Y. Takeda, N. Imanishi, O. Yamamoto, J. Electrochem. Soc. 147 (2000) 1671.
[21] C. Chang, P.N. Kumta, J. Power Sources 75 (1998) 44.
[22] M. Winter, J.O. Besenhard, Electrochim. Acta 45 (1999) 31.
[23] A.A. Anani, S. Crouch-Baker, R.A. Huggins, J. Electrochem. Soc. 135 (1998) 2103.
[24] J. Wang, I.D. Raistrick, R.A. Huggins, J. Electrochem. Soc. 133 (1986) 457.
[25] S.C. Nam, C.H. Paik, W.I. Cho, B.W. Cho, H.S. Chun, K.S. Yun, J. Power Sources 84 (1999) 24.
[26] T. Brousse, R. Retoux, U. Herterich, D.M. Schleich, J. Electrochem. Soc. 145 (1998) 1.
[27] J. Li, H. Li, Z. Wang, X. Huang, L. Chen, J. Power Sources 81 (1999) 346.
[28] R. Retoux, T. Brousse, D.M. Schleich, J. Electrochem. Soc. 146 (1999) 2472.
[29] W. Liu, X. Huang, Z. Wang, H. Li, L. Chen, J. Electrochem. Soc. 145 (1998) 59.
[30] J.Y. Kim, D.E. King, P.N. Kumta, G.E. Blomgren, J. Electrochem. Soc. 147 (2000) 4411.
[31] S.C. Nam, Y.S. Yoon, W.I. Cho, B.W. Cho, H.S. Chun, K.S. Yun, Electrochem. Commun. 3 (2001) 6.